Investigation of the interface behavior of a viscous fluid under free surface shear flow using an eccentric transparent Couette cell

Prashanth Thirunavukkarasu, Francis Fournier, Arnaud Pignolet, Romain Castellani, Céline Cohen, Edith Peuvrel-Disdier, Rudy Valette, Bruno Vergnes

Investigation of the interface behavior of a viscous fluid under free surface shear flow using an eccentric transparent Couette cell

Prashanth THIRUNAVUKKARASU[1,2], Francis FOURNIER[1], Arnaud PIGNOLET[1], Romain CASTELLANI[1], Céline COHEN[3], Edith PEUVREL-DISDIER[1*], Rudy VALETTE[1], Bruno VERGNES[1].

[1] Mines Paris, PSL University, Centre for material forming (CEMEF), UMR CNRS, 06904 Sophia Antipolis, France.

[2] Manufacture Française des Pneumatiques Michelin – Ladoux, 63118 Cébazat, France.

[3] Université Côte d'Azur, CNRS UMR 7010, Institut de Physique de Nice, Parc Valrose, 06108 Nice, France.

* Corresponding author: Edith PEUVREL-DISDIER
edith.peuvrel-disdier@minesparis.psl.eu

Abstract

In the present work, a prototype was developed to observe the flow behavior of viscous fluids under free surface shear and determine an adhesion energy in this flow geometry. The geometry consists in an eccentric Couette cell (an outer cylinder radius of 89.5 mm, an inner cylinder radius of 43,75 mm and a minimal gap of 3 mm) that can be used in two modes, where both cylinders can respectively rotate in the same or opposite directions. Cylinders are horizontal and short relatively to their diameters (30 mm long). Transparent windows allow *in-situ* flow observations. The design, development, and testing of the prototype with a model viscous fluid (silicone fluid with a 2.2 10^4 Pa.s Newtonian viscosity) are reported in this paper.

The flow behavior of small fluid volumes (fill factor smaller than 15%) was investigated under co- and counter-rotating configurations to determine steady-state flow conditions. Stationary conditions were identified in the counter-rotating mode. The velocity conditions and resulting observations are studied and analysed. However, the viscous fluid of the study (silicone fluid) presents a unilateral contact with the cylinder surfaces and no adhesion energy contribution could be detected.

Keywords: Free surfaces, Couette cell, Viscous flow, Interfacial flow.

1. Introduction

As a fluid moves across a solid surface, three different types of interfacial flows are encountered: i) the flow at solid/fluid interfaces, dealing with slip and no slip boundary conditions, ii) the flow at solid/fluid/air interfaces, i.e. contact line, dealing with the dynamics of contact lines, and iii) the flow along the fluid/air interfaces or free surfaces. The present work aims at developing a transparent flow geometry to investigate the dynamics of contact lines and the shape of free surfaces in the case of viscous fluids under shear flow.

The motion of contact lines is a ubiquitous situation encountered in nature and technological applications (e.g. sticking of rain drops on solid surfaces) and many industrial processes in relation with wetting and spreading phenomena (surface coating, painting). The study of the dynamics of contact lines originated in the early 20th century (West, 1911; Lucas, 1918; Washburn, 1921, Rideal, 1922; Blake and Haynes, 1969; Voinov, 1976; De Gennes, 1985; Cox, 1986) and has remained an open research area (see e.g., Lu et al., 2016; Terhemen and Gbaoron, 2020; Andreotti and Snoeijer, 2020; Chamakos et al., 2020). The first studies on the motion of contact lines of a fluid were conducted under capillary pressure (West, 1911). The movement of a fluid volume over a solid substrate appeared to be complex from a physico-chemical point of view, due to the necessity of a multiscale description of the fluid at the contact line (see e.g. De Gennes, 1985; Bonn et al., 2009; Lu et al., 2016). From a mechanical point of view, the motion of the contact line over a solid surface violates the no slip boundary condition and leads to a stress singularity (Huh and Scriven, 1971; Wilson et al., 2006; Chamakos et al., 2020). Most of the works were conducted in the case of simple liquids and low viscosity fluids (< 10 Pa.s) where the surface tension plays a role in the force balance at the interface. However, in the case of viscous fluids, the flow is dominated by viscous forces with potential viscous dissipation phenomena. In this case, weaker forces, such as e.g. surface tension, might be neglected.

During polymer processing, an understanding of the complex fluid flow and the thermomechanical description of the processing conditions is crucial to control the final properties of the material. To better understand this complex flow behavior, direct observations across transparent walls of processing equipments were conducted in the second half of the 20th century. For example, front transparent walls were introduced in internal mixers to observe the mixing process (in particular the distributive mixing) of highly viscous polymers, and to identify zones of stagnation depending on the rotor geometry (Freakley and Wan Idris, 1979; Asai et al., 1983; Min and White, 1985; White et al., 1986; Min, 1987). Simplified flow

conditions were used to investigate the efficiency of the rotor geometry by using a single rotor rotating in a transparent cylindric chamber (Breuer et al., 2005). Interfacial flows were investigated in transparent dies with different geometries at the exit of extruders to understand the slip behaviour, flow regimes, and flow instabilities (Robert et al., 2004; Combeaud et al., 2004). Transparent walls in injection moulding allowed to observe the kinematics of the fountain flow during the filling process, where the shear flow of the front free surface is driven by the pressure (Poiseuille flow) (Yokoi, 2009).

Simple flow geometries such as transparent Couette cells (including eccentric ones) were used to investigate the kinematics of distributive mixing (Chaiken et al., 1986; de Haas et al., 1998; Agassant et al., 2009). This flow geometry was also extensively studied to understand the journal bearing flow (de Haas et al., 1998). These observations were conducted on model fluids (room temperature, low viscosity less than 10 Pa.s) and on a fully filled chamber which did not allow the observation of free surfaces nor contact lines.

Eccentric (or off-centred) Couette cells, when filled at small fluid volumes, can be used to study the behavior at the fluid/gas interface in the thin gap zone between the cylinders. This flow configuration was used to simulate the coating process of a solid substrate by a fluid in roll coating applications and to investigate printer's instabilities which develop at the interface (Rabaud et al., 1990; Pan and de Bruyn, 1994; Varela Lópeza et al., 2002).

The present work reports on the design and development of a transparent eccentric Couette cell dedicated to viscous fluids (> 10^3 Pa.s) where both cylinders can rotate independently. In this study, the objective was to investigate the flow behavior of a small fluid volume near the thin flow gap region (smallest gap between the cylinders and region of maximum shear). This paper reports on the preliminary observations with the prototype with a viscous silicone fluid, at room temperature, in co- and counter-rotating conditions. The behaviour of the fluid is described as a function of the volume, the relative directions, and velocities between the inner and outer cylinders. Stationary flow configurations favourable to observe the interfacial flow behavior at contact lines and free surfaces are determined. The stationary conditions in the counter-rotating mode are more particularly investigated.

2. Description of the prototype

2.1. Experiments principle

The eccentric Couette cell was chosen as it provides a localized zone of high shear rate around the thin gap region, in comparison to classical Couette cells with a uniform shear rate. The fluid motion is induced by the rotation of the two independent cylinders capable of rotating in both directions with different speeds. We focussed our attention on small fluid volumes to observe free surfaces and contact lines in the thin gap region, where the flow is simple and well defined. With a change in the fluid volume, two flow configurations can be observed in co- and counter-rotating modes (illustrated in the latter mode on Figure 1):

- below a critical fluid volume (referred as $\mathcal{V}_{h0}$ thereafter and corresponding to the minimum volume to form a continuous layer of thickness h_0 on the outer cylinder surface), the fluid volume is in direct contact with both cylinders (Figure 1.a) and the dynamics of 4 contact lines (indicated by letters A, B, C and D) and 2 free surfaces (depicted as arcs $\widehat{AB}$ and $\widehat{CD}$) can be observed. In the counter-rotating mode, A and C are receding contact lines, whereas B and D are advancing contact lines;
- above this critical fluid volume, a thin uniform layer of fluid of thickness h_0 is formed along the outer cylinder while the remaining fluid volume is recirculated in the upstream direction. The recirculating volume is in contact with the inner cylinder (indicated as A) and with the fluid layer (indicated as B). Here, two contact lines with the surface of the inner cylinder indicated as A and C and one free surface can be observed.

Insert Figure 1

2.2. Design and description of the device

The Couette cell was designed to work with viscous fluids (as high as 5.10^4 Pa.s) and can be heated to temperatures up to 100°C. The originality of the prototype is to allow the flow of viscous fluids to be observed *in-situ* in a confined geometry by the rotation of the independently rotating cylinders. A global view of the Couette cell and auxiliary elements is shown in Figure 2. The auxiliary systems of the Couette cell are:

- a heating system consisting of two independent heat transfer fluid circuits for the cylinders,
- a computer interface to control the motors and record the parameters,
- a joystick to control the rotation of the cylinders via the interface,
- a recording system consisting of a camera and supplementary lighting.

Insert Figure 2

The outer cylinder radius (R_1 = 89.5 mm) was chosen to provide a large zone of observation in the thin gap region. The radii of outer and inner cylinders were chosen with a ratio of nearly 2:1 (R_2 = 43.75 mm). The thin flow gap h_0 can be varied from 3 to 11 mm. In this study, we work with a 3 mm gap to provide a higher shear in at the thin flow gap. The depth of the chamber w (equal to the length of the cylinders, 30 mm) was chosen to facilitate the observation of free surfaces without distortion of the image and minimize the effect of drag by the transparent walls during shear flow (estimation for h_0 = 3 mm and a constant outer cylinder speed (Agassant et al., 2017)). The present Couette cell depth is similar to the chamber depth of small laboratory internal mixers.

The outer cylinder surface is welded to the device and cannot be disassembled. On the other hand, the inner cylinder surface can be replaced allowing us to change its nature (composition, roughness, etc.). In this paper, we will present the results obtained with similar cylinder (inner and outer) surfaces, made of 42Cd4 steel with similar roughness. Observations of the fluid flow are performed by the transmission of light through two transparent windows. They are made of annealed borosilicate glass to withstand high stresses and temperatures. The front transparent window is circular. The rear one is annular in shape to accommodate the inner cylinder rotation axis. The windows are held in place on either side of the outer cylinder by ring flanges and screws and thus rotate at the same speed as the outer cylinder. The introduction of the fluid and the cleaning steps are achieved by dis- and re-assembling the front window. The flow observations are recorded with a Panasonic G80 camera (equipped with an all-purpose Panasonic 12-60 zoom lens or Olympus 30 mm macro) and with the help of supplementary lighting.

The inner and outer cylinders are heated by closed circuit flows of heat transfer fluid (commercial silicone oil, Julabo™ 8940114 (Julabo, Seelbach, Germany)) connected to two independent thermal baths. Each cylinder surface temperature is measured by a thermocouple inserted in the heat transfer fluid circulation. A third thermocouple can be inserted in a hole through the front window to control the fluid temperature at the end of the experiment. Cylinders are driven by independent brushless motors (MDP enterprise, Neyron, France). The maximum torque provided by each motor is respectively 100 Nm (120 rpm maximum) and 50 Nm (85 rpm maximum) for the outer and inner cylinders. The torque on each motor axis is measured via a 100 mm lever arm and a stress gauge. Initial observations were carried out on a limited range of rotational speeds, +/- 16 and +/- 3.2 rpm for the inner and outer cylinders respectively, providing a maximum theoretical shear rate of 35 s^{-1} in the counter-rotating mode

with the current configuration. The rotational speeds and directions of the cylinders are imposed and controlled by software and/or manually by a joystick. Data measured by the sensors are displayed and recorded with the help of a program developed in LabVIEW.

Thus, this prototype permits the observation and investigation of the flow behavior of viscous fluids with the possibility of varying i) the fluid volume, ii) the fluid used, iii) the temperature of the fluid during flow, iv) the nature of the inner cylinder surface, v) the roughness of the inner and outer cylinder surfaces, vi) the nature of the transparent windows, vii) the minimal gap h_0, viii) the cylinder rotation speeds, and ix) the cylinder rotation directions. In this paper, the fluid volume, the cylinder speeds and rotation directions are varied while fixing the other parameters. Some limitations of the flow geometry are described in the Appendix.

2.2. Fluid characteristics

A transparent viscous silicone fluid (commercially sold as Liquid Glass Thinking Putty®, Crazy Aaron, Nebraska, USA, with a density of 0.992 g/cm^3, supplier data) was selected for the flow experiments. Its rheological behavior was measured by dynamic rheometry on an ARES (TA Instruments, Germany). The viscosity curve follows a classical Carreau-Yasuda behavior, characterized by a 2.2 10^4 Pa.s Newtonian viscosity, a power law index of 0.36, a relaxation time of 0.86 s and a Yasuda parameter of 0.69. Flow experiments were conducted at room temperature in the present work.

3. Results and discussion

3.1 Fluid volumes of interest

Two fluid volumes of interest (depicted in Figure 1) are determined based on geometrical considerations:

- There is a critical volume ($\mathcal{V}_{h0}$) delimiting the two configurations depicted in Figure 1. It is defined as the minimum volume to form a continuous layer of thickness h_0 on the outer cylinder surface, when the fluid is driven through the thin gap h_0. It represents 8.7% of the free volume of the present Couette geometry. At volumes smaller than the critical volume ($\mathcal{V} \leq \mathcal{V}_{h0}$), the flow configuration is similar to Figure 1.a. in the counter-rotating mode, the fluid can be stabilized between the two-cylinder surfaces in the upstream direction. At very

small volume (below 4.5% of the cell free volume), the fluid is difficult to stabilize because the volume is too small to fill the chamber width;

- At volumes larger than the critical volume ($\mathcal{V} \geq \mathcal{V}_{h0}$), the flow is like the condition of Figure 1b, with a continuous uniform layer and a recirculating volume;
- The study is restricted to volumes below 15 % of the free volume of the present Couette geometry, corresponding to a uniform layer and a recirculating fluid limited to the converging zone of the geometry. Figure 1 is a good illustration of the maximum volume in this study.

The objective is to determine the steady state flow conditions in which the contact lines and free surfaces can be observed at fixed locations (in relation to the laboratory framework). With this objective in mind, the first step of the work was to explore different flow conditions while varying the fluid volume, the rotation direction of the cylinders and their velocities. The steady state conditions in the counter-rotating mode are more particularly investigated and results are presented in a second step.

3.2 Co-rotation conditions

The fluid volume is first introduced by dismantling the front transparent window. In order to determine the stabilization conditions, the outer cylinder speed is first set constant. The speed of the inner cylinder is then progressively increased. The fluid volume behavior under shear with free surfaces is observed for each velocity condition to determine whether the flow is stationary or not. The same procedure is repeated for different outer cylinder speeds. Linear speeds $\overrightarrow{V_1}$, and $\overrightarrow{V_2}$ of the cylinders are considered thereafter to describe the flow conditions. Subscripts 1 and 2 refer to the outer and inner cylinders, respectively.

In the case of a small fluid volume ($\mathcal{V} < \mathcal{V}_{h0}$), the situation is always nonstationary. The fluid is deformed as it passes through the converging flow channel. This results in the formation of a film of uniform thickness h_0 on the outer cylinder surface which length is defined by the introduced volume and the minimal gap.

In the case of a large fluid volume ($\mathcal{V} > \mathcal{V}_{h0}$), in addition to the continuous layer of thickness h_0, a recirculating volume is formed at the entrance of the converging zone (Figure 3) as observed in some coating (Rabaud et al., 1990) or calendaring processes (Agassant et al., 2017). The fluid volume in this zone is controlled by the introduced volume, the minimal gap

and the relative cylinders speeds. The recirculating volume progressively decreases with time. The situation is nonstationary except when $|\overrightarrow{V_2}| \ll |\overrightarrow{V_1}|$, condition for a steady state flow.

Insert Figure 3

3.3 Counter-rotating conditions

For a given outer cylinder speed ($\overrightarrow{V_1}$) and fluid volume, the fluid can be stabilised over a range of inner cylinder speeds [$\overrightarrow{V_{2_{min}}}$, $\overrightarrow{V_{2_{max}}}$] in counter-rotating conditions. The minimum inner cylinder speed required for stabilisation depends on the fluid properties. The procedure is repeated at different outer cylinder speeds to investigate the corresponding minimum inner cylinder speeds required for stationary flows. We focussed our attention on the determination of the couple ($\overrightarrow{V_1}, \overrightarrow{V_{2_{min}}}$) for steady state condition. This stationary condition is referred as ($\overrightarrow{V_1}, \overrightarrow{V_2}$) for sake of simplicity afterwards.

Three types of flow conditions can be observed in the case of a small fluid volume ($\mathcal{V} < \mathcal{V}_{h0}$), when increasing the inner cylinder velocity ($\overrightarrow{V_2}$), at a fixed outer cylinder velocity ($\overrightarrow{V_1}$).

- When the inner cylinder velocity is small compared to the outer cylinder one ($|\overrightarrow{V_2}| < |\overrightarrow{V_1}|$), it is impossible to stabilize the fluid. The fluid is dragged along the outer cylinder surface until it is split into two blocks at the exit of the thin gap region (Figure 4.a);
- In an optimal range of inner cylinder velocity, with $|\overrightarrow{V_2}| > |\overrightarrow{V_1}|$, the fluid can be stabilized between the cylinder surfaces in the converging zone (Figure 4.b), allowing steady state observations. While its position is stabilized between the cylinders, the volume is subjected to a rolling motion;
- At higher inner cylinder velocities ($|\overrightarrow{V_2}| >> |\overrightarrow{V_1}|$), the flow is dominated by the inner cylinder rotation and the fluid is dragged by the inner cylinder surface. The fluid volume adopts a cylindric shape as it is displaced away from the thin gap region. At this position, the fluid rotates and loses contact with the outer cylinder surface (Figure 4.c).

Insert Figure 4

While working with a large fluid volume ($\mathcal{V} > \mathcal{V}_{h0}$), a uniform layer is deposited on the outer cylinder surface. As in the co-rotating mode, a recirculating fluid volume is observed at the entrance of the converging zone in addition to the uniform layer. This volume is mainly fixed by the initial fluid volume, the minimum gap h_0 and the cylinder speeds. Two flow conditions

can be distinguished for the recirculating volume depending on the inner cylinder velocity ($\overrightarrow{V_1}$ being fixed):

- For $0 \leq |\overrightarrow{V_2}| < |\overrightarrow{V_2}_{max}|$, the recirculating volume (Figure 5.a) is stabilized at the thin gap region. Steady state observations are possible when the inner cylinder velocity does not dominate the flow. The recirculating volume depends on the relative cylinders speeds;
- At higher inner cylinder velocities ($|\overrightarrow{V_2}| >> |\overrightarrow{V_1}|$), the recirculating volume gets separated from the uniform layer and progressively dragged away by the inner cylinder surface from the thin gap region (Figure 5.b). As for the small fluid volume at high $\overrightarrow{V_2}$, the recirculating volume tends to form a cylinder rotating between the inner cylinder and the uniform deposited layer.

Insert Figure 5

Among the steady state observations, the flow observations in the counter-rotating mode for a small fluid volume ($\mathcal{V} < \mathcal{V}_{h0}$) are more interesting for two reasons:

- the stabilized condition is achieved due to the flow geometry and the fluid rheological response;
- they allow the observation of four contact lines with two receding ones (indicated with letters A and C in Figure 1.a) and two advancing ones (letters B and D).

Hence, the steady state conditions in the counter-rotating mode are more particularly investigated.

3.4 Analysis of the stabilized conditions in the counter-rotating mode

Stabilized conditions were first characterized via the applied cylinder velocities ($\overrightarrow{V_1}, \overrightarrow{V_2}$), $\overrightarrow{V_2}$ being the minimum inner cylinder velocity to stabilize the flow for a fixed $\overrightarrow{V_1}$ (as introduced in paragraph 3.3). The evolution of the minimum inner cylinder velocity $|\overrightarrow{V_2}|$ necessary to stabilize the fluid volume versus the imposed outer cylinder velocity $|\overrightarrow{V_1}|$ is depicted in Figure 6 for different fluid volumes.

Insert Figure 6

Irrespective of the fluid volume, the inner cylinder velocity $|\overrightarrow{V_2}|$ appears to vary linearly with the outer one $|\overrightarrow{V_1}|$. The ratio $|\overrightarrow{V_2}|/|\overrightarrow{V_1}|$ appears to be constant, around 1.3. A stabilization at equal

linear velocities ($\left|\overrightarrow{V_1}\right|/\left|\overrightarrow{V_2}\right| = 1$) would be expected if there was no drag effect of the transparent windows, i.e. in case of stationary transparent windows. In the present geometry, the glass windows are rotating at the same velocity as the outer cylinder. A higher velocity must thus be provided to the inner cylinder to overcome the combined drag of the outer cylinder and the transparent walls on the fluid.

Under stabilized and transient flow conditions, the shape of the deformed volume (lateral cross section) can be determined (Figure 7), allowing one to derive different characteristic dimensions of the fluid volume under the free surface shear flow (shape of the free surfaces, location of contact lines, interfacial surfaces between the fluid and the walls). However, it is observed that, once stationary conditions are provided, the fluid can be stabilized at different positions in the converging part of the flow channel. Figure 8 illustrates two extreme stabilization positions for the same fluid volume and velocity conditions. The mean shear rate experienced by the fluid and the shape of the stabilized volume depend on the local geometry of the flow channel. The dimensions of the stabilized volume (interfacial lengths between the fluid and the cylinder, $\widehat{AB}$ and $\widehat{CD}$, and free surfaces lengths, $\widehat{BC}$ and $\widehat{DA}$, measured on the lateral projection, see Figure 7.b, same notation as in Figure 1.a) first depend on the volume and on the position where it is stabilized, but not on the imposed velocities.

Insert Figure 7

Insert Figure 8

Streamlines can also be observed when shearing a new silicone sample (thanks to the presence of internal tracers, see Appendix), illustrated on Figure 7.a. As mentioned before, when the fluid is subjected to stationary conditions in the counter-rotating mode, the volume is recirculating between the cylinder surfaces (figure 7.a). However, the rotation of the transparent windows generates a 3D flow. The complex 3D shape of the recirculating volume is easier to observe once the flow is stopped and the fluid is extracted (Figure 9). The complex shape, as observed from the top (Figure 9.c), is due to the imposed opposite drag flows (plus potential distortion during the extraction and flow under gravity). The thicker part (see Figures 9.b-c) presents an expected curved shape whereas the thinner part results from the drag induced by the rotation of the glass windows. The complex 3D shape of the stabilized volume can also be seen on the lateral view via differences in contrast in the central zone (focused zone, corresponding to the contact area of the fluid with the front transparent window, and a less focused zone around (Figure 7.a)).

Insert Figure 9

4 Conclusions

The characterization of the interfacial flow behavior of viscous fluids still remains an open topic. Experimental observations of the interfacial flow are important to understand this behavior, especially for viscous fluids. A transparent eccentric Couette cell, with independently rotating cylinders, was designed and developed to characterize the flow of viscous fluids under controlled shear with free surfaces.

The prototype provides transient and steady state flow observations by controlling the direction and rotation speed of the cylinders. The behavior of a viscous silicone fluid was investigated at room temperature while varying the direction of rotation of the cylinders (co- or counter-rotation), the speed of the inner and outer cylinders, and the introduced fluid volume. The paper focuses on the presentation of the prototype, its different functionalities, steady state flow observations and the required conditions for these observations.

Different flow conditions allowing to stabilize the fluid volume in the converging zone (close to the minimal gap) were identified:

- for a small fluid volume, the volume could be stabilized in the counter-rotating mode, forming a recirculating volume at a certain range of inner and outer cylinder velocities;
- for a larger volume with a continuous uniform layer of fluid on the outer cylinder, a recirculating fluid volume could be stabilized whatever the cylinder velocities in the co-rotating mode and under defined velocity conditions in the counter-rotating mode.

The conditions for the stabilization of a small volume in the counter-rotating mode were analysed. The additional drag due to the rotation of the transparent windows results in a complex 3D flow. The recirculating volume is found to be stabilized at different positions in the converging zone even for similar velocity conditions. Its dimensions are mainly fixed by the channel geometry and the introduced volume, and not by the imposed velocity conditions.

The flow configuration was designed to estimate the adhesion energy under free surface shear conditions. Flow conditions of interest were determined. However, the viscous fluid of the study (silicone fluid) presents a unilateral contact with the cylinder’s surfaces. A next step could be to consider the flow behaviour of a viscous adhesive fluid in the counter-rotating mode in transient and stationary conditions experimentally and by numerical simulation to determine if an effect of the adhesion energy could be detected in the case of a viscous fluid. It would also

be interested to investigate the flow behaviour of other fluids such as yield stress fluids, suspensions, in the present flow geometry.

Acknowledgements

The authors wish to thank Marc Bouyssou, Eric Brotons, Christelle Combeaud, Guillaume Corvec, Gilbert Fiorucci for their involvement in the manufacturing of the different components of the machine. Special thanks are addressed to Bruno Dratz and Pascal Tremblay from the Michelin company for their initiative, involvement, and discussions during the work.

Funding

This study was carried out within the framework of the OSUM project, FUI AAP23, funded by BPiFrance. Thirunavukkarasu's PhD was funded by Michelin MFP and a CIFRE grant from the French agency Association Nationale de la Recherche et de la Technologie (A.N.R.T.).

Appendix: Limitations of the flow geometry

Some limitations were identified while working with the prototype:

- with the present configuration of motors, 5.10^4 Pa.s appears to be an upper limit of the fluid viscosity that can be sheared in the thin gap region without breakage risks for glass windows.
- Despite routine cleaning, tiny fluid volumes tend to get trapped at the interfaces between the mobile and immobile parts (e.g., between the rear window and the central immobile part) or between mobile parts (e.g., between the windows and the inner cylinder sides, see Figure A(b)). The presence of these impurities leads, under shear, to the loss of transparency of the fluid over time (illustrated in Figure A). It was verified that this loss of transparency due to impurities did not influence the rheological behavior of the fluid.
- The fluid volume slightly varies over time during shear with the continuous entrapment and release of the fluid trapped in the different tiny gaps of the flow geometry.

Insert Figure A

References

Agassant, J.F., Poitou, A. and Valette, R., “A kinematic approach to distributive mixing” in Mixing and Compounding of Polymers, 2nd edition, Manas Zloczower, I. (Ed.), Carl Hanser Hanser, Munich, p 217-240 (2009)

Agassant, J.F., Avenas, P., Carreau, P.J., Vergnes, B. and Vincent, M., “Polymer Processing - Principle and Modelling”, Carl Hanser Verlag, Munich (2017), DOI: 10.3139/9781569906064

Andreotti, B. and Snoeijer, J.H., “Statics and dynamics of soft wetting”, Ann. Rev. Fluid Mech., 52, 285-308 (2020), DOI: 10.1146/annurev-fluid-010719-060147

Asai, T., Fukui, T., Inoue, K. and Kuriyama, M., Proc. International Rubber Conference Paper III-4, Paris (1983)

Blake, T. D. and Haynes, J. M. “Kinetics of liquid displacement”. J. Colloid Interface Sci. 30(3), 421-423 (1969) DOI: 10.1016/0021-9797(69)90411-1

Bonn, D., Eggers, J., Indekeu, J., Meunier, J. and Rolley, E., “Wetting and spreading”, Rev. Mod. Phys., 81, 739-805 (2009), DOI: 10.1103/RevModPhys.81.739

Breuer, O., Chen, H., Lin, B. and Sundararaj, U., “Simulation and visualization of flow in a new miniature mixer for multiphase polymer systems”, J. Appl. Polym. Sci., 97, 136–142 (2005), DOI: 10.1002/app.20998

Chaiken, J., Chevray, R., Tabor, M. and Tan, Q. M., “Experimental study of Lagrangian turbulence in a Stokes flow”, Proc. Roy. Soc., A 408, 165-174 (1986), DOI: 10.1098/rspa.1986.0115

Chamakos, N.T., Sema, D.G. and Papathanasiou, A.G., “Progress in modeling wetting phenomena on structured substrates”, Arch. Comput. Meth. Eng., (2020), DOI: 10.1007/s11831-020-09431-3

Combeaud, C., Demay, Y. and Vergnes, B., “Experimental study of the volume defects in polystyrene extrusion”, J. Non-Newt. Fluid Mech., 121, 175-185 (2004), DOI: 10.1016/j.jnnfm.2004.06.007

Cox, R. G. “The dynamics of the spreading of liquids on a solid surface. Part 1. Viscous flow”. J. Fluid Mech., 168, 169-194 (1986), DOI: 10.1017/S0022112086000332

de Gennes, P.G., “Wetting: statics and dynamics”, Rev. Mod. Phys., 57(3), 827-863 (1985), DOI: 10.1103/RevModPhys.57.827

de Haas, K.H., van den Ende, D., Blom, C., Altena, E.G., Beukema, G.J. and Mellema, J. “A counter-rotating Couette apparatus to study deformation of a sub-millimeter sized particle in shear flow”. Rev. Scient. Instr., 69 (3), 1391-1397 (1998). DOI: 10.1063/1.1148771

Freakley, P.K. and Wan Idris, W.Y., “Visualization of flow during the processing of rubber in an internal mixer”, Rubber Chem. Technol., 52, 134-145 (1979). DOI: 10.5254/1.3535197

Huh, C. and Scriven, L.E., “Hydrodynamic model of steady movement of a solid / liquid / fluid contact line”, J. Colloid Interf. Sci., 35, 85-101 (1971), DOI: 10.1016/0021-9797(71)90188-3

Lu, G., Wang, X.D. and Duan, Y.Y., “A critical review of dynamic wetting by complex fluids: from Newtonian fluids to non-Newtonian fluids and nanofluids”, Adv. Colloid Interface Sci., 236, 43–62 (2016), DOI: 10.1016/j.cis.2016.07.004

Lucas, R., “Über das Zeitgesetz des kapillaren Aufstiegs von Flüssigkeiten”, Koll.-Z., 23, 15-22 (1918)

Min, K. and White, J.L., “Flow visualization of the motions of elastomers and molten plastics in an internal mixer”, Rubber Chem. Technol., 58, 1024-1037 (1985), DOI: 10.5254/1.3536098

Min, K., “Flow visualization parallel and perpendicular to the rotor axes for elastomers and molten plastics in an internal mixer - The influence of rotor design”, Intern. Polym. Proc., 1, 179-187 (1987), DOI: 10.3139/217.870179

Pan, L. J. and de Bruyn, R., “Spatially uniform travelling cellular patterns at a driven interface”, Phys. Rev., E 49, 483-493 (1994), DOI: 10.1103/PhysRevE.49.483

Rabaud, M., Michalland, S. and Couder, Y., “Dynamical regimes of directional viscous fingering: Spatiotemporal chaos and wave propagation”, Phys. Rev. Lett. ,64, 184-189 (1990), DOI: 10.1103/PhysRevLett.64.184

Rideal, E.K., “On the flow of liquids under capillary pressure”, Phil. Mag., 44, 1152-1159 (1922). DOI: 10.1080/14786441008634082

Robert, L., Demay, Y., Vergnes, B., “Stick-slip flow of high density polyethylene in a transparent slit die investigated by laser Doppler velocimetry”, Rheol. Acta, 43, 89-98 (2004), DOI:10.1007/s00397-003-0323-x

Terhemen, T.A. and Gbaoron, Y.S., “Contact angle hysteresis – Advantages and disadvantages: A critical review”, Rev. Adhes. Adhes., 8, 47-67 (2020), DOI: 10.7569/RAA.2020.097302

Varela López a, F., Paucharda, L., Rosenb, M. and Rabaud, M., “Non-Newtonian effects on ribbing instability threshold”, J. Non-Newt. Fluid Mech., 103, 123–139 (2002). DOI: 10.1016/S0377-0257(01)00165-3

Voinov, O.V., “Hydrodynamics of wetting”, Fluid dynamics, 11, 714-721 (1976), DOI: 10.1007/BF01012963

Washburn, E.W., “The dynamics of capillary flow”, Phys. Rev., 17 (3), 273-283 (1921), DOI 10.1103/PhysRev.17.273

West, G. D., “On the resistance to the motion of a thread of mercury in a glass tube”, Proc. Roy. Soc., A 86, 20-25 (1911). DOI: 10.1098/rspa.1911.0076

White, J.L., Min, K., Ma, C.Y. and Brzoskowski, R., “Basic studies of flow visualization of processing of elastomers and their compounds: Internal mixer and extrusion”, J. Polym. Eng., 6, 79-93 (1986). DOI: 10.1515/POLYENG.1986.6.1-4.79

Wilson, M.C.T., Summers, J.L., Shikhmurzaev, Y.D., Clarke, A. and Blake, T.D., “Non-local hydrodynamic influence on the dynamic contact angle: Slip models vs experiment”, Phys. Rev. E, 73(4), 041606 (2006), DOI: 10.1103/PhysRevE.73.041606

Yokoi, H., “Part IV: Process visualization, control, optimization, and simulation: Internal visualization of mold cavity and heating cylinder”, in Injection Molding, Technology and Fundamentals, Kamal, M.R., Isayev, A. and Liu, S.-J. (Eds.), Carl Hanser Verlag, Munich, p 395-438 (2009), DOI: 10.3139/9783446433731

Figure captions

Figure 1: Schematic representation of the flow in stationary regime in the case of the counter-rotating mode for (a) a small volume of fluid $\mathcal{V} < \mathcal{V}_{h0}$ and (b) a large volume $\mathcal{V} > \mathcal{V}_{h0}$,. ω refers to the rotational velocity of the cylinders, subscripts 1 and 2 referring to the outer and inner cylinder respectively. h_0 denotes the minimal gap.

Figure 2: Couette cell and its environment: 1. Computer interface control, 2. Outer cylinder surface, 3. Inner cylinder surface, 4. Observation zone between the cylinder's surfaces, 5. Heat transfer fluid connections, 6. Joystick to drive the cylinders rotation direction and their velocities 7. Power control and motor variators.

Figure 3: Flow observation of a large fluid volume $\mathcal{V} > \mathcal{V}_{h0}$ in co-rotation condition.

Figure 4: Flow observations of a small fluid volume $\mathcal{V} < \mathcal{V}_{h0}$ in the counter-rotating mode for a fixed outer cylinder velocity $\overrightarrow{V_1}$ at: (a) an insufficient inner cylinder velocity $\overrightarrow{V_2}$ ($|\overrightarrow{V_2}| < |\overrightarrow{V_1}|$), (b) optimal inner cylinder velocity for stabilization ($|\overrightarrow{V_2}| > |\overrightarrow{V_1}|$), (c) excess inner cylinder velocity ($|\overrightarrow{V_2}| >> |\overrightarrow{V_1}|$).

Figure 5: Flow observations of a large fluid volume $\mathcal{V} > \mathcal{V}_{h0}$ in the counter-rotating mode for a fixed outer cylinder velocity at: (a) a sufficient inner cylinder velocity, (b) an excess inner cylinder velocity ($|\overrightarrow{V_2}| >> |\overrightarrow{V_1}|$).

Figure 6: Stabilized flow conditions in the counter-rotating mode for different fluid volumes: Minimum required inner cylinder velocity for stabilization $|\overrightarrow{V_2}|$ as a function of the imposed outer cylinder velocity $|\overrightarrow{V_1}|$. Fluid volumes are indicated as introduced masses of fluid.

Figure 7: Illustration of streamlines under stabilized conditions (a) and contour image analysis of the flow outline (b) for a 20 g sample stabilized in the counter-rotating mode at $|\overrightarrow{V_1}|$ = 9.4 mm/s, $|\overrightarrow{V_2}|$. = 14.3 mm/s. Letters A to D indicate contact lines (same notation as in Figure 1.a).

Figure 8: Extreme positions of stabilization for a similar fluid volume (8 g) at the same velocity conditions $|\overrightarrow{V_1}|$ = 18.7 mm/s, $|\overrightarrow{V_2}|$. = 21.5 mm/s in the counter-rotating mode.

Figure 9: a. Lateral view (*xy* plane) of the stabilized volume in the counter-rotating mode before the flow stops. The arrows represent the flow direction before flow is stopped, b. Dewetting of

the fluid volume from the inner cylinder surface by inversing the direction of rotation of the outer cylinder, c. Top-view (*yz* plane) of the fluid volume after extraction.

Figure A: Illustration of the loss of transparency of the fluid over time during shear flow

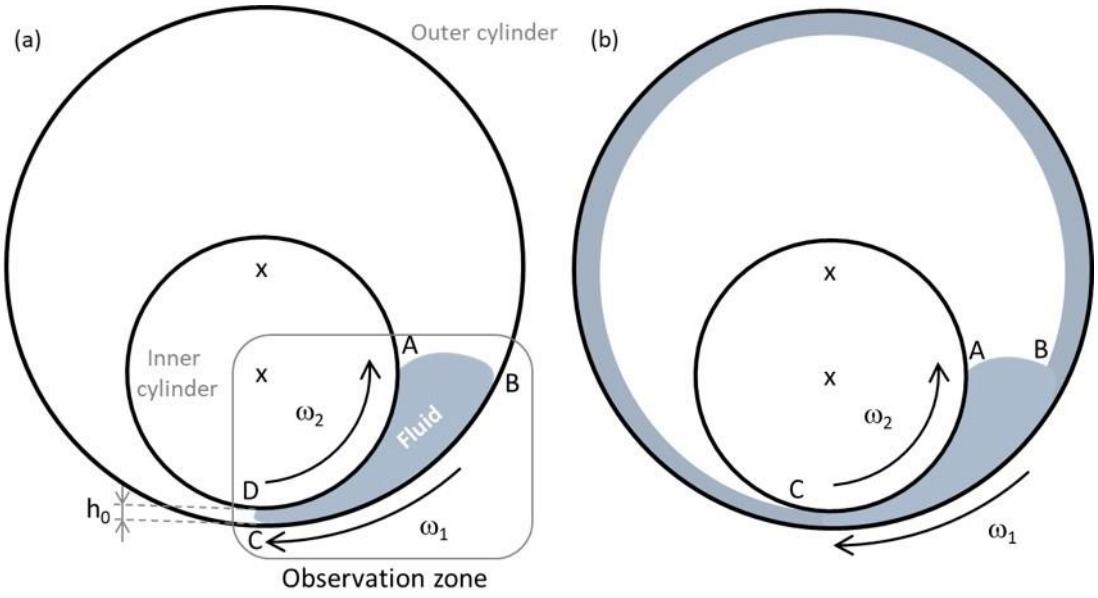

Figure 1: Schematic representation of the flow in stationary regime in the case of the counter-rotating mode for (a) a small volume of fluid $\mathcal{V} < \mathcal{V}_{h0}$ and (b) a large volume $\mathcal{V} > \mathcal{V}_{h0}$. ω refers to the rotational velocity of the cylinders, subscripts 1 and 2 referring to the outer and inner cylinder respectively. h_0 denotes the minimal gap.

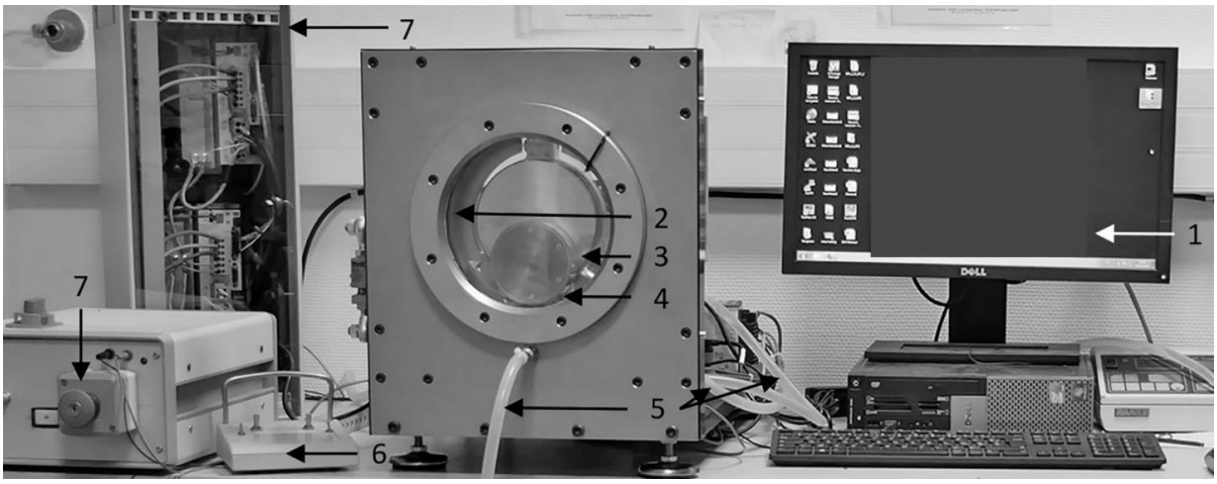

Figure 2: Couette cell and its environment: 1. Computer interface control, 2. Outer cylinder surface, 3. Inner cylinder surface, 4. Observation zone between the cylinders surfaces, 5. Heat transfer fluid connections, 6. Joystick to drive the cylinders rotation direction and their velocities 7. Power control and motor variators.

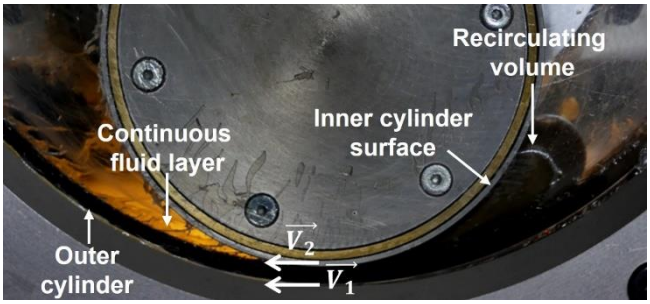

Figure 3: Flow observation of a large fluid volume $\mathcal{V} > \mathcal{V}_{h0}$ in co-rotation condition.

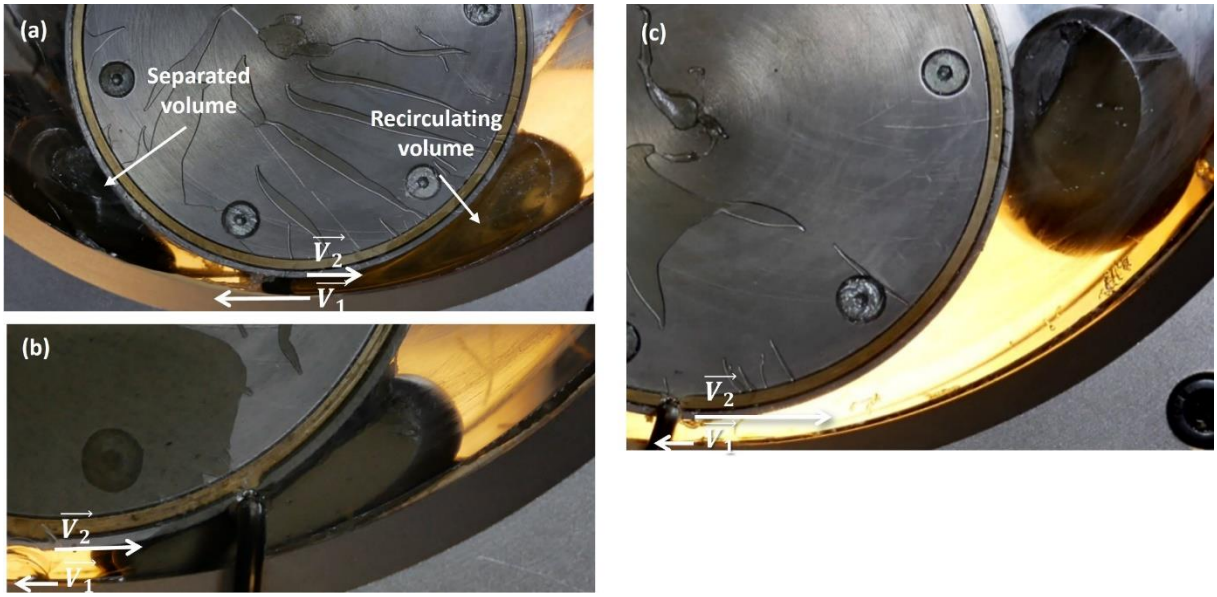

Figure 4: Flow observations of a small fluid volume $\mathcal{V} < \mathcal{V}_{h0}$ in the counter-rotating mode for a fixed outer cylinder velocity $\overrightarrow{V_1}$ at:

(a) an insufficient inner cylinder velocity $\overrightarrow{V_2}$ ($|\overrightarrow{V_2}| < |\overrightarrow{V_1}|$), (b) optimal inner cylinder velocity for stabilization ($|\overrightarrow{V_2}| > |\overrightarrow{V_1}|$), (c) excess inner cylinder velocity ($|\overrightarrow{V_2}| >> |\overrightarrow{V_1}|$).

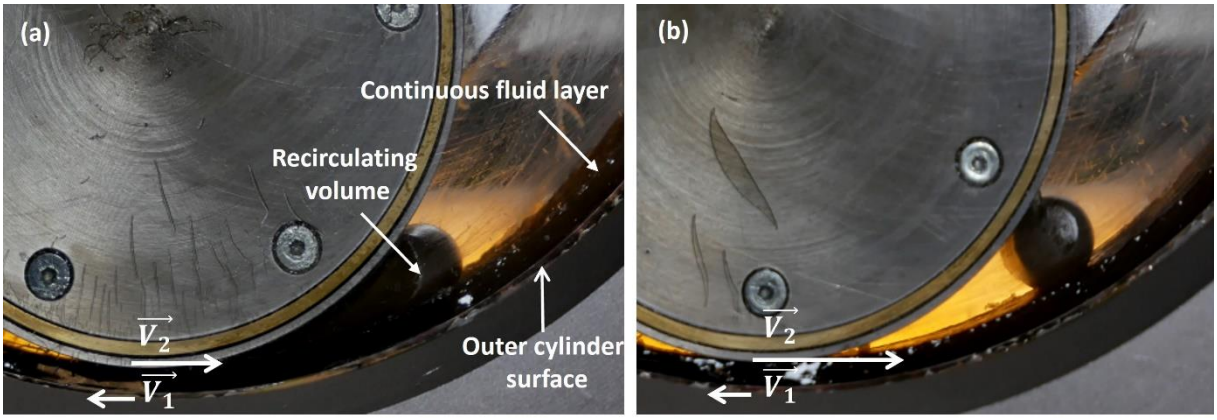

Figure 5: Flow observations of a large fluid volume $\mathcal{V} > \mathcal{V}_{h0}$ in the counter-rotating mode for a fixed outer cylinder velocity at: (a) a sufficient inner cylinder velocity, (b) an excess inner cylinder velocity ($|\overrightarrow{V_2}| >> |\overrightarrow{V_1}|$).

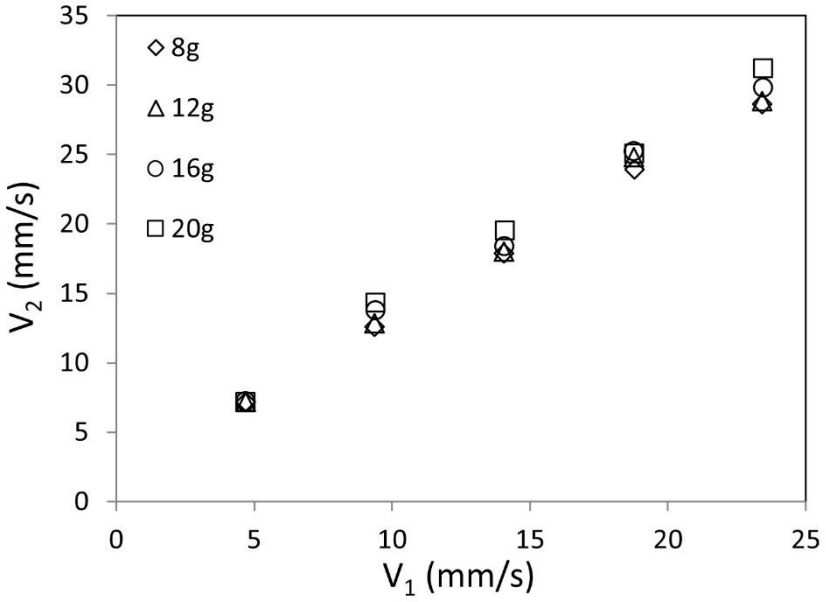

Figure 6: Stabilized flow conditions in the counter-rotating mode for different fluid volumes: Minimum required inner cylinder velocity for stabilization $\left|\overrightarrow{V_2}\right|$ as a function of the imposed outer cylinder velocity $\left|\overrightarrow{V_1}\right|$. Fluid volumes are indicated as introduced masses of fluid.

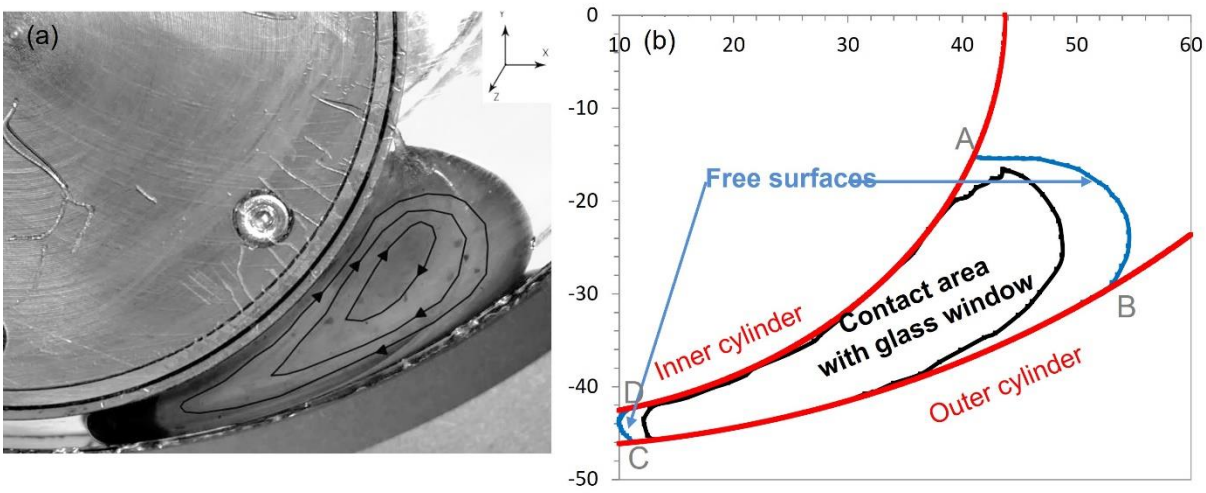

Figure 7: Illustration of streamlines under stabilized conditions (a) and contour image analysis of the flow outline (b) for a 20 g sample stabilized in the counter-rotating mode at $|\overrightarrow{V_1}|$ = 9.4 mm/s, $|\overrightarrow{V_2}|$. = 14.3 mm/s. Letters A to D indicate contact lines (same notation as in Figure 1.a).

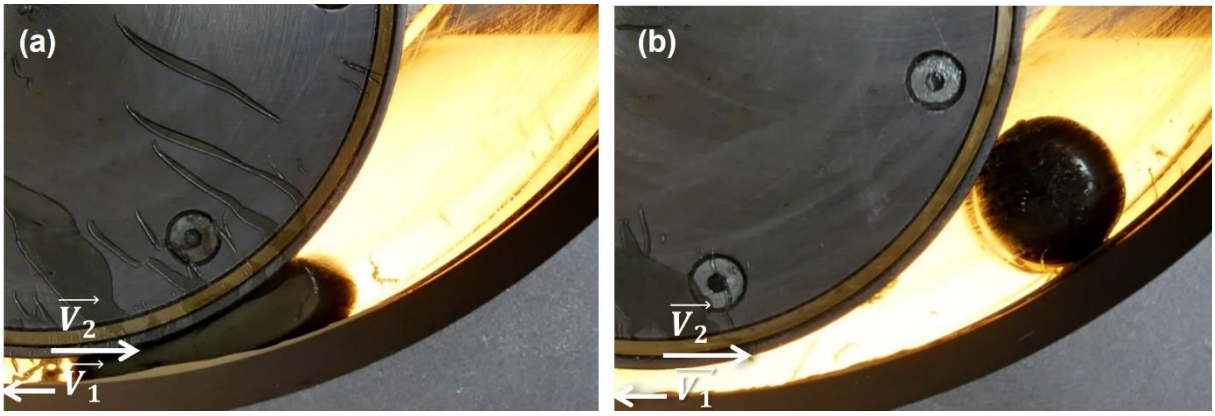

Figure 8: Extreme positions of stabilization for a similar fluid volume (8 g) at the same velocity conditions $|\overrightarrow{V_1}|$ = 18.7 mm/s, $|\overrightarrow{V_2}|$. = 21.5 mm/s in the counter-rotating mode.

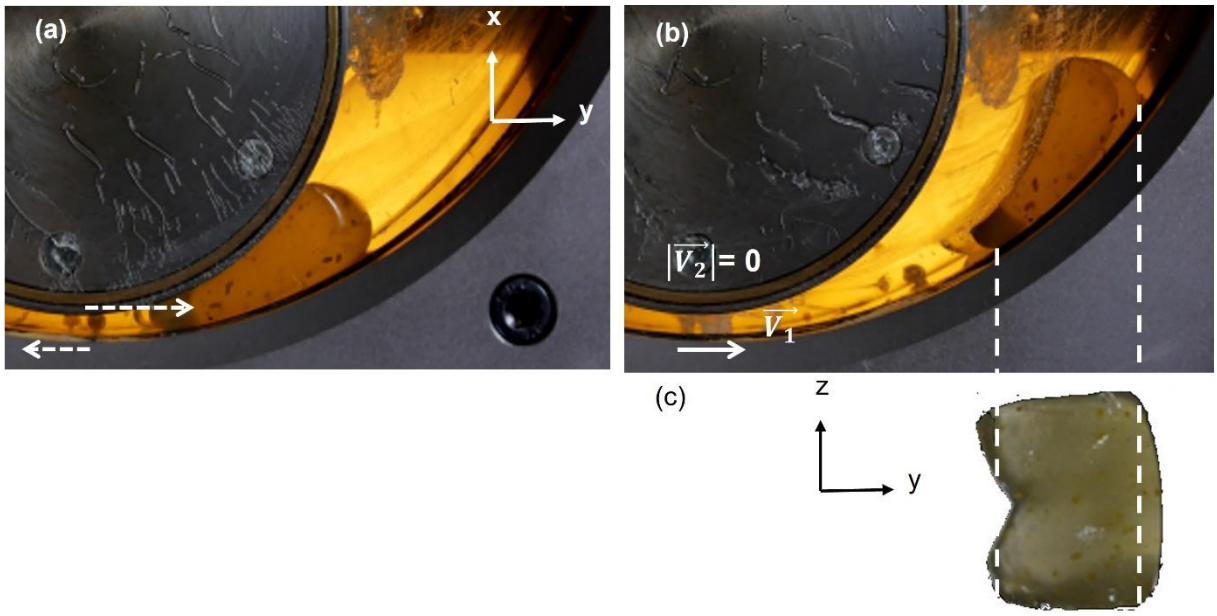

Figure 9: a. Lateral view (*xy* plane) of the stabilized volume in the counter-rotating mode before the flow stops. The arrows represent the flow direction before flow is stopped, b. Dewetting of the fluid volume from the inner cylinder surface by inversing the direction of rotation of the outer cylinder, c. Top-view (*yz* plane) of the fluid volume after extraction.

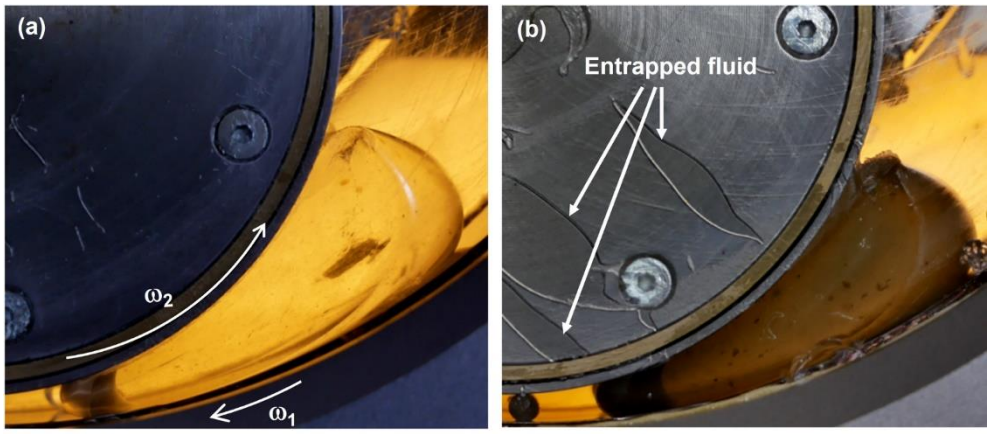

Figure A: Illustration of the loss of transparency of the fluid over time during shear flow